ARTICLE

doi:10.1038/nature10360

Neocortical excitation/inhibition balance in information processing and social dysfunction

Ofer Yizhar[1,2]*, Lief E. Fenno[1,3]*, Matthias Prigge[4], Franziska Schneider[4], Thomas J. Davidson[1], Daniel J. O'Shea[1,3], Vikaas S. Sohal[1,5], Inbal Goshen[1], Joel Finkelstein[1], Jeanne T. Paz[6], Katja Stehfest[4], Roman Fudim[4], Charu Ramakrishnan[1], John R. Huguenard[6], Peter Hegemann[4] & Karl Deisseroth[1,7,8,9]

Severe behavioural deficits in psychiatric diseases such as autism and schizophrenia have been hypothesized to arise from elevations in the cellular balance of excitation and inhibition (E/I balance) within neural microcircuitry. This hypothesis could unify diverse streams of pathophysiological and genetic evidence, but has not been susceptible to direct testing. Here we design and use several novel optogenetic tools to causally investigate the cellular E/I balance hypothesis in freely moving mammals, and explore the associated circuit physiology. Elevation, but not reduction, of cellular E/I balance within the mouse medial prefrontal cortex was found to elicit a profound impairment in cellular information processing, associated with specific behavioural impairments and increased high-frequency power in the 30–80 Hz range, which have both been observed in clinical conditions in humans. Consistent with the E/I balance hypothesis, compensatory elevation of inhibitory cell excitability partially rescued social deficits caused by E/I balance elevation. These results provide support for the elevated cellular E/I balance hypothesis of severe neuropsychiatric disease-related symptoms.

The neurophysiological substrates of most psychiatric disorders are poorly understood, despite accumulating information on genetic factors associated with complex behavioural phenotypes such as those observed in autism and schizophrenia[1–4]. One emerging principle is that a range of seemingly unrelated genetic abnormalities can give rise to the same class of psychiatric phenotype (such as social behaviour dysfunction)[5], highlighting the need to identify simplifying circuit-level concepts[6–8] that could unify diverse genetic factors under a common pathophysiological principle. One such hypothesis is that elevation in the ratio of cortical cellular excitation to inhibition (cellular E/I balance), for example through increased activity in excitatory neurons or reduction in inhibitory neuron function, could give rise to the social and cognitive deficits observed in diseases such as autism[6,7,9,10]. This hypothesis would unify diverse streams of pathophysiological evidence[11–15], including the suggestion that many autism-related genes are linked to gain-of-function phenotypes in ion channels and synaptic proteins[16], that the autistic state is associated with hyperactivity in frontal brain regions[17–19] with elevated high-frequency cortical oscillations[20,21] and that ~30% of autistic patients show clinically apparent seizures[22,23]. However, it is not clear if such an imbalance would impart its disease-relevant effects by influencing development[9,10,24] or real-time function; moreover, the hypothesis has been neither directly testable nor universally accepted[25–27], although much pioneering work[8–30] may have a bearing on this question.

Although the motivations for social interaction may vary among species, a common theme (independent of motivation) is that social interactions are challenging owing to high levels of uncertainty, and can require rapid interpretation of complex social stimuli to inform the moment-to-moment generation, refinement and selection of models for the actions of other individuals. Social behaviour assays for experimental mammals such as mice are available, as well as optogenetic methods for direct causal testing of hypotheses regarding the role of activity in specified neuronal populations[31,32]. Using optogenetics, selectively favouring excitation of one population over another (for example with a bistable step-function opsin (SFO), which can depolarize neurons for prolonged periods[33,34]) could address the E/I balance hypothesis, but membrane depolarizations induced by known SFOs[33,35] are not sufficiently stable after a single light flash over the period required for complex behavioural testing. Nor has it been possible thus far to independently excite multiple cell groups within the same volume of tissue, important for testing aspects of the balance hypothesis. Potential strategies exist to manipulate independent neuronal populations in the context of known potent blue-light-activated (~460 nm peak) excitatory tools[36], but currently available redshifted channelrhodopsins are not suitable for combinatorial control because redshifts of less than 50 nm[37,38] do not translate into separable channels of control *in vivo*, and the most redshifted channelrhodopsin (>70 nm; VChR1) suffers from low expression levels and weak photocurrents[39].

To enable combinatorial interrogation of E/I balance in experimental animals, we therefore first created several novel optogenetic tools: a series of chimaeric redshifted opsins comprised of sequences from ChR1[40] and VChR1[39], and a stable SFO operative over the 30 min timescale. We then directly tested the E/I balance hypothesis by optogenetically elevating cellular E/I balance in medial prefrontal

[1]Department of Bioengineering, W083 Clark Center, 318 Campus Drive West, Stanford University, Stanford, California USA. [2]Department of Neurobiology, Weizmann Institute of Science, Rehovot 76100, Israel. [3]Neuroscience Program, W083 Clark Center, 318 Campus Drive West, Stanford University, Stanford, California 94305, USA. [4]Institute of Biology, Experimental Biophysics, Humboldt-Universität, Invalidenstraße 42, D-10115 Berlin, Germany. [5]Department of Psychiatry, University of California, San Francisco, San Francisco, California 94143, USA. [6]Department of Neurology and Neurological Science, W083 Clark Center, 318 Campus Drive West, Stanford University, Stanford, California 94305, USA. [7]Howard Hughes Medical Institute, W083 Clark Center, 318 Campus Drive West, Stanford University, Stanford, California 94305, USA. [8]Department of Psychiatry and Behavioral Sciences, W083 Clark Center, 318 Campus Drive West, Stanford University, Stanford, California 94305, USA. [9]CNC Program, W083 Clark Center, 318 Campus Drive West, Stanford University, Stanford, California 94305, USA.
*These authors contributed equally to this work.

cortex (mPFC) during behaviours relevant for social function and learning in freely moving mice.

Development of a stabilized SFO

We first sought to generate an SFO suitably stable for mammalian behaviour. We hypothesized that combining previously characterized SFO mutations (C128S[33] and D156A[35]), both shown to confer minute-scale deactivation kinetics, would synergistically stabilize the open channel state. We generated and purified from *Pichia pastoris* the ChR2 mutants C128S, D156A and C128S/D156A (Supplementary Fig. 1a) to measure intrinsic open-state stability in the absence of potentially confounding cellular properties. Time-resolved spectroscopy to measure photocycle progression showed expected rapid absorbance changes with light delivery that largely recovered within several minutes for single mutants C128S (Fig. 1a) and D156A (Fig. 1b). In contrast, the double mutant C128S/D156A showed remarkable stability of the activated state, with little detectable return to the dark state even after 30 min (Fig. 1c and Supplementary Fig. 1b). We next performed whole-cell recordings from neurons expressing this construct (Supplementary Fig. 1c). Consistent with spectroscopic observations, neurons expressing ChR2(C128S/D156A) gave rise to far more stable photocurrents than those induced by either single mutant[33,35] (Fig. 1d). A spontaneous deactivation time constant of 29 min was observed for ChR2(C128S/D156A) ($r^2 = 0.91$), 4.2-fold longer than D156A (6.9 min, $r^2 = 0.83$) (Fig. 1e). Peak photocurrents in neurons expressing ChR2(C128S/D156A) or ChR2(D156A) were comparable (231.08 ± 31.19 pA; $n = 9$ cells and 320.96 ± 78.26 pA; $n = 7$ cells, respectively; $P = 0.26$). The double mutant could be deactivated with either 590 or 405 nm light (Fig. 1f, g and Supplementary Fig. 1d, e). We refer to the double-mutant gene and protein as the stable SFO (SSFO).

As slow channelrhodopsins enable transduced cells to act as photon integrators across time[33], we hypothesized that the SSFO would enable photoactivation with extremely low light power. Indeed, intensities as low as 8 μW mm^{-2} generated hundreds of picoamperes of whole-cell photocurrent in neurons expressing SSFO (Fig. 1h). Photocurrent amplitude increased with monoexponential kinetics during illumination (Fig. 1h, left) whereas activation time constants were linearly dependent on activation power on a log–log scale until the channel-intrinsic millisecond-scale activation time constant (τ_{on}) was approached (Fig. 1h, middle; $n = 27$ recordings from 5 cells). The total number of photons required for photocurrents to reach a fixed fraction of I_{max} was constant over many orders of magnitude of light power (Fig. 1h, right; $9.1 \times 10^8 \pm 1.6 \times 10^8$ photons; $n = 27$ recordings from 5 cells). Taken together, these data indicate that SSFO acts as an integrator with photocurrent determined by total photon exposure.

Consequences of altered E/I balance

To validate the SSFO *in vivo*, we performed optrode recordings[41] in anaesthetized mice expressing SSFO in prelimbic and infralimbic subregions of the mPFC. To modulate excitation, we used adeno-associated virus (AAV) expressing SSFO–EYFP (EYFP, enhanced yellow fluorescent protein) under control of the CaMKIIα promoter (CaMKIIα::SSFO; Supplementary Methods). To modulate inhibition we expressed a double-floxed inverted open-reading-frame (DIO) AAV[32] encoding SSFO–EYFP in PV::Cre (PV, parvalbumin) transgenic mice (PV::SSFO), where expression of SSFO–EYFP is restricted to GABAergic PV neurons[32] (Supplementary Fig. 2). Using extracellular

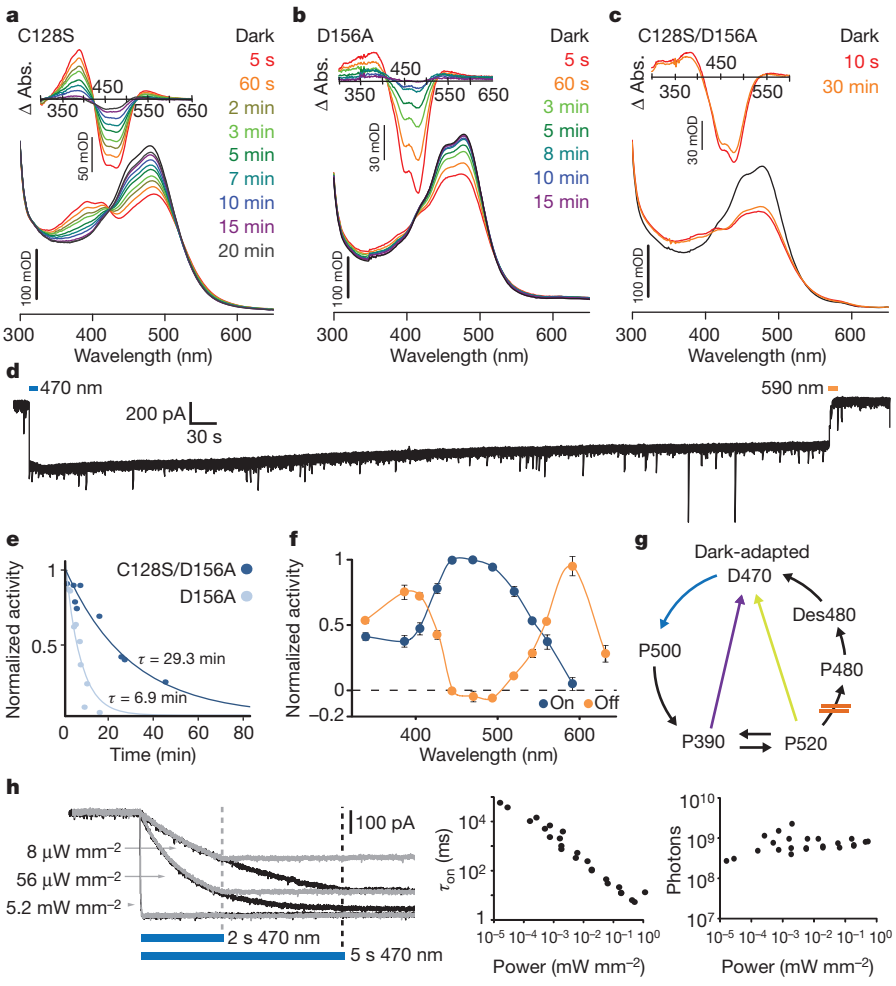

Figure 1 | Kinetic and absorbance properties of a stabilized SFO. **a–c**, Absorption spectra recorded after illumination with 450 nm light for 30 s. Absorption difference spectra (Δ Abs.) taken from the corresponding absorption spectra are shown in the insets. Spectra were collected at the indicated times after the end of illumination; note prominent recovery after 3 min in the single mutants, in contrast to the double mutant. **d**, Representative whole-cell patch-clamp recording of photocurrent in a cultured hippocampal neuron expressing ChR2(C128S/D156A) SSFO. Blue and orange bars indicate activation and deactivation light pulses. **e**, Monoexponential fits of photocurrent decay in cells expressing ChR2(C128S/D156A) (dark blue; $\tau = 29$ min) or ChR2(D156A) (light blue; $\tau = 6.9$ min). **f**, Activation (blue) and deactivation (orange) spectra recorded from cultured neurons expressing ChR2(C128S/D156A). **g**, Simplified photocycle scheme; in C128/D156 mutants the transition P520 to P480 is probably slowed down or blocked, avoiding the desensitized state Des480 which cannot be reactivated with 470 nm light. Both yellow and violet light (yellow and violet arrows) shuttle the channels to an inactive state (see Supplementary Fig. 1). **h**, Whole-cell photocurrent responses of a cultured neuron expressing SSFO to 470 nm light pulses of indicated power (left). Pulse lengths were 2 s (grey traces) or 5 s (black traces). Dashed lines mark light pulse termination. Apparent time constants for activation (τ_{on}) are shown on a log–log plot versus light power ($n = 27$ recordings from 5 cells; middle). Within this broad range of light power, the calculated number of incident photons arriving at each cell for photocurrents to reach the exponential curve constant (63% of I_{max}) for that cell was constant (right). Each point represents a photon number from a single recording at a given light power.

recordings in anaesthetized mice to access this medial structure, we observed significant light-induced changes in multiunit activity restricted to transduced regions of the mPFC (Supplementary Fig. 3). In mice expressing CaMKIIα::SSFO, multiunit spike rates increased within the transduced area as expected (Supplementary Fig. 3b, c, e, f). Conversely, in PV::SSFO mice (despite the sparseness of PV cells and incomplete transduction; Supplementary Fig. 2), multiunit activity profoundly decreased after an identical 1 s pulse of 473 nm light and returned to near-baseline levels after a 2 s 561 nm pulse (Supplementary Fig. 3b, d, e; subsequent behavioural work described later used identical opsin-expression experimental conditions). We next examined the effects of altered E/I balance on prefrontal information transmission using whole-cell patch-clamp recordings. In the presence of ongoing synaptic activity, CaMKIIα::SSFO activation increased synaptic input onto both expressing and non-expressing pyramidal cells (Supplementary Fig. 4a, b). To test the input–output relationship, we stimulated CaMKIIα::SSFO neurons with trains of simulated excitatory post-synaptic currents (sEPSCs) designed to span a wide range of sEPSC rates over time[32] (Supplementary Fig. 4c and Supplementary Methods). Elevation of the cellular E/I balance in these slices by activation of CaMKIIα::SSFO led to saturation of the input–output (*I–O*) curve and a reduction in *I–O* mutual information (Supplementary Fig. 4d–i). In contrast, activation of SSFO in PV cells potently reduced ongoing synaptic activity (Supplementary Fig. 5a) and decreased *I–O* curve gain in recorded pyramidal cells, as expected via synaptic inhibition. However, the shape of the *I–O* curve was preserved with only a small reduction in dynamic range but no change in saturation and no significant effect on *I–O* mutual information (Supplementary Fig. 5b–g). Overall, the reduction in principal neuron information throughput after light activation in CaMKIIα::SSFO slices was 4.8-fold larger than in PV::SSFO slices ($P = 0.0144$; across a wide range of analysis parameters, Supplementary Fig. 5h). These results indicate that at the principal neuron level, information processing may be more impaired by increased E/I balance.

We next examined the effects of this elevated cellular E/I balance on behaviour. We expressed SSFO in either mPFC excitatory or inhibitory PV-expressing neurons as described earlier, and implanted a chronic fibre-optic connector terminating dorsal to the mPFC (Fig. 2a, b). We confirmed, using c-Fos staining as a marker of activity, that in the awake state neural activity could be increased or decreased by activation of SSFO in pyramidal and PV neurons respectively (Fig. 2c and Supplementary Fig. 6a). In behavioural tests, all mice received a single 2 s pulse of 473 nm light through the implanted fibre-optic connector, followed by removal of the fibre optic 1 min before introduction into the behavioural chamber, capitalizing on the stability of the SSFO. Exploration of a new same-sex juvenile introduced to the experimental animal home cage was virtually abolished in the elevated E/I (CaMKIIα::SSFO) group following SSFO activation (Fig. 2d and Supplementary Videos 1 and 2; $n = 8$ CaMKIIα::SSFO mice and $n = 6$ controls; $P < 0.0005$); PV::SSFO mice showed no effect of

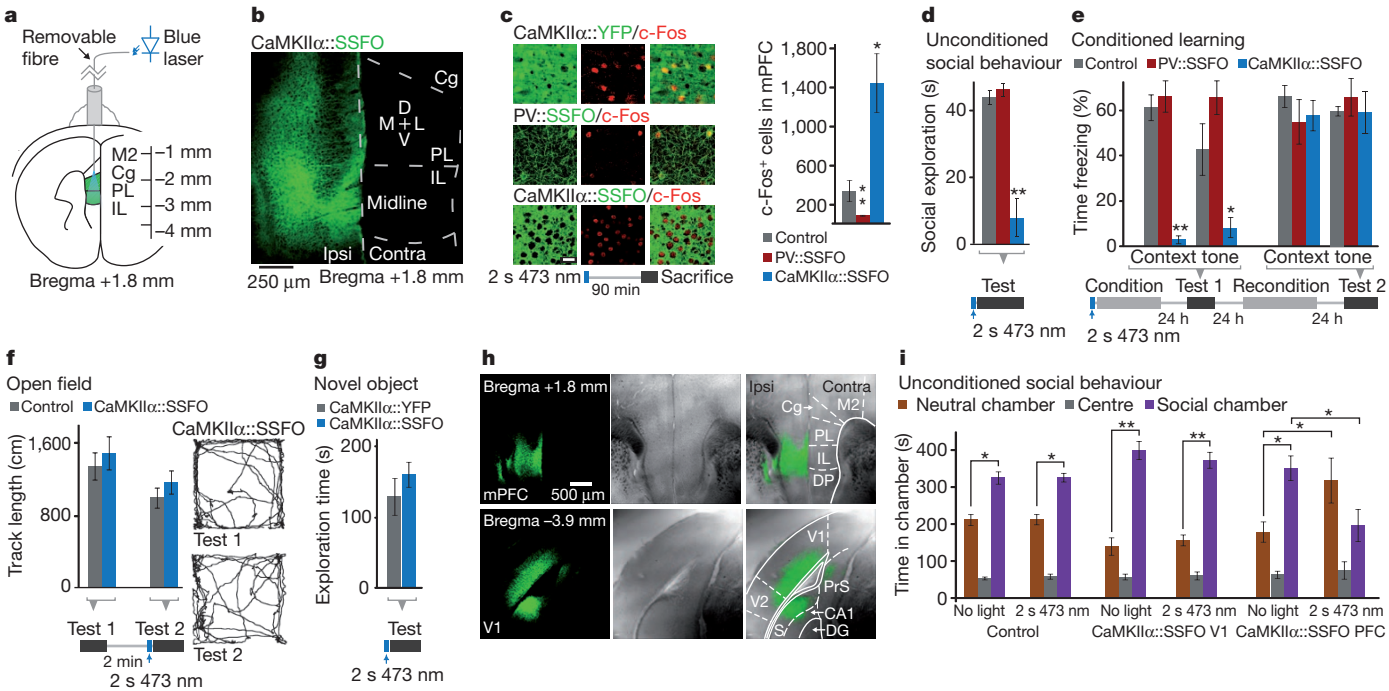

Figure 2 | Elevated, but not reduced, prefrontal E/I balance leads to behavioural impairment. **a**, Experimental setup for behavioural experiments. Green region marks viral injection area; fibre-optic connector was attached to the light guide only transiently before testing. Cg, cingulate cortex; IL, infralimbic cortex; M2, secondary motor cortex; PL, prelimbic cortex. **b**, Confocal image from a mouse injected with CaMKIIα::SSFO–EYFP virus shows expression in prelimbic and infralimbic cortex. D, dorsal; L, lateral; M, medial; V, ventral. Contra, contralateral; Ipsi, ipsilateral. **c**, Representative images of prefrontal slices from PV::SSFO and CaMKIIα::SSFO mice stained for c-Fos 90 min after a 2 s 473 nm light pulse. Scale bar, 25 µm. Graph shows average c-Fos-positive cell counts in the mPFC of control, CaMKIIα::SSFO and PV::SSFO mice. **d**, Social exploration in control, CaMKIIα::SSFO and PV::SSFO mice of a juvenile intruder in the home cage. CaMKIIα::SSFO mice showed a significant reduction in social exploration. **e**, Mice administered one 2 s 473 nm pulse of light before fear conditioning were tested the next day for freezing in response to the conditioned context or auditory cue; CaMKIIα::SSFO mice were significantly impaired in freezing responses to both conditioned stimuli. On the following day, mice were reconditioned without optical stimulation and freezing was evaluated 24 h later. All mice showed similar freezing behaviour in the absence of light. **f**, Open-field exploration in CaMKIIα::SSFO (blue) and CaMKIIα::EYFP (grey) mice, before (Test 1) and after (Test 2) light activation. Example tracks from a CaMKIIα::SSFO mouse are shown. **g**, Novel object exploration over a 10 min period is similar in mice expressing CaMKIIα::SSFO (blue) and CaMKIIα::EYFP (grey). **h**, Phase contrast and fluorescence images of coronal sections from wild-type mice injected with CaMKIIα::SSFO in PFC (top) or V1 (bottom). **i**, Social behaviour in the three-chamber test is impaired following a 2 s 473 nm light pulse in mice expressing CaMKIIα::SSFO in the PFC ($n = 5$), but not in control mice ($n = 6$) or in mice expressing CaMKIIα::SSFO in V1 ($n = 8$). Time spent in a given chamber after stimulation is only significantly altered in mice expressing CaMKIIα::SSFO. All bar graphs depict mean ± s.e.m. (*$P < 0.05$, **$P < 0.005$).

SSFO activation (Fig. 2d; $n = 6$ PV::SSFO mice; $P > 0.1$). To test episodic learning (also impaired in autism and schizophrenia[42,43]), we next subjected the same mice to a fear conditioning protocol immediately following SSFO activation. The elevated E/I (CaMKIIα::SSFO) mice showed no conditioned responses 24 h after conditioning (Fig. 3e; to either context, $P < 0.0005$; or tone, $P < 0.05$, compared with controls). We then reconditioned the same mice in the absence of light activation of SSFO. Twenty-four hours later, responses of these mice were indistinguishable from controls (Fig. 2e; $P > 0.1$ cue and context). The reduced E/I balance (PV::SSFO) group showed no significant impairment compared with controls to either tone or context (Fig. 2e; $P = 0.09$ and $P = 0.56$, respectively). Elevated E/I balance-induced deficits were not a result of motor impairment as, in the same mice, open-field behaviour was normal (Fig. 2f and Supplementary Fig. 6b; $n = 8$ CaMKIIα::SSFO mice and $n = 6$ CaMKIIα::EYFP mice; Supplementary Fig. 8d shows unchanged immediate foot-shock response in CaMKIIα::SSFO mice). Additionally, CaMKIIα::SSFO mice showed no abnormalities in exploration of a novel object (Fig. 2g; $n = 8$ CaMKIIα::SSFO and $n = 10$ CaMKIIα::EYFP mice; $P = 0.47$).

We next examined whether the social impairment induced by altered E/I balance could arise in any cortical region. We tested three groups of mice: CaMKIIα::SSFO virus in the mPFC, as earlier ($n = 5$; Fig. 2h, top); control virus in the mPFC ($n = 6$); and CaMKIIα::SSFO virus in the primary visual cortex (Fig. 2h, bottom; V1 area 17; $n = 8$), an area in which microstimulation generates potent internal visual stimuli[44]. These mice were tested in the three-chamber social exploration paradigm[45], an independent measure of social interaction. We found that control mice and CaMKIIα::SSFO V1 mice preferred the chamber with a novel conspecific mouse, in both no-light and light conditions (Fig. 2i). In contrast, CaMKIIα::SSFO mPFC mice exhibited normal social exploration at baseline, but significantly reduced social exploration after SSFO activation (Fig. 2i). This impairment in social behaviour was not correlated with an increased-anxiety phenotype in the elevated plus maze (Supplementary Fig. 6d). Viral targeting was evaluated post-hoc and revealed CaMKIIα::SSFO expression in targeted regions in all mice tested (Fig. 2h and Supplementary Fig. 7). Taken together, these experiments indicate that elevated, but not reduced, cellular E/I balance in the mPFC significantly impairs social behaviour and conditioning, and that this deficit does not result from changes in anxiety or locomotion.

E/I balance elevation elicits rhythmic activity

Behavioural impairment in both autism and schizophrenia has been associated with elevated baseline (non-evoked) high-frequency activity in the 30–80 Hz range[20,21,46]. To examine the activity patterns in awake behaving mice during E/I balance modulation, we designed a chronic multi-site optrode (CMO; Fig. 3a and Methods) to sample activity both in modulated mPFC and in unmodulated regions above and below the mPFC. We hypothesized that temporal stability and photon integration of SSFO would allow light delivery with superficial (non-brain penetrating) fibre-optic placement (Supplementary Fig. 8a, b), and verified that superficial light delivery could modulate SSFO-expressing mPFC cells using c-Fos quantification and behavioural testing (Supplementary Fig. 8c–e). We used CMOs to record neural activity in CaMKIIα::SSFO mice; fibre placement was superficial and electrode positions were confirmed post-hoc by electrolytic lesioning (Fig. 3b). We found that CaMKIIα::SSFO mice with CMO implants had normal baseline social behaviour that was impaired after a 1 s 473 nm pulse (Fig. 3c; $n = 3$, $P = 0.044$). Novel object exploration was unaffected by stimulation, consistent with previous findings (Fig. 3c; $P = 0.82$). The activation pulse did not significantly alter locomotor behaviour in either the home cage (not shown) or a novel open field, although the latter trended towards reduced anxiety (Supplementary Fig. 8f and Supplementary Video 3).

We recorded multiunit activity and local field potentials simultaneously on all channels during these behaviour trials. In the home cage, we observed significant increases in multiunit activity after a 1 s 473 nm light pulse in channels within the SSFO-expressing regions (Supplementary Fig. 8g, h; 77 ± 18% on modulated channels, compared with −3.4 ± 4.4% on unmodulated channels; $n = 4$ modulated and 4 unmodulated channels in 3 mice averaged over 4 sweeps per mouse; $P = 0.02$). Modulated channels showed a marked increase in high-frequency activity with a peak at 80 Hz after SSFO activation (Fig. 3e) delimited to the activation period (Fig. 3d, e, left). Channels with increased high-frequency activity had concomitant reduction of lower frequencies (Fig. 3e, right, inset). High-frequency activity was

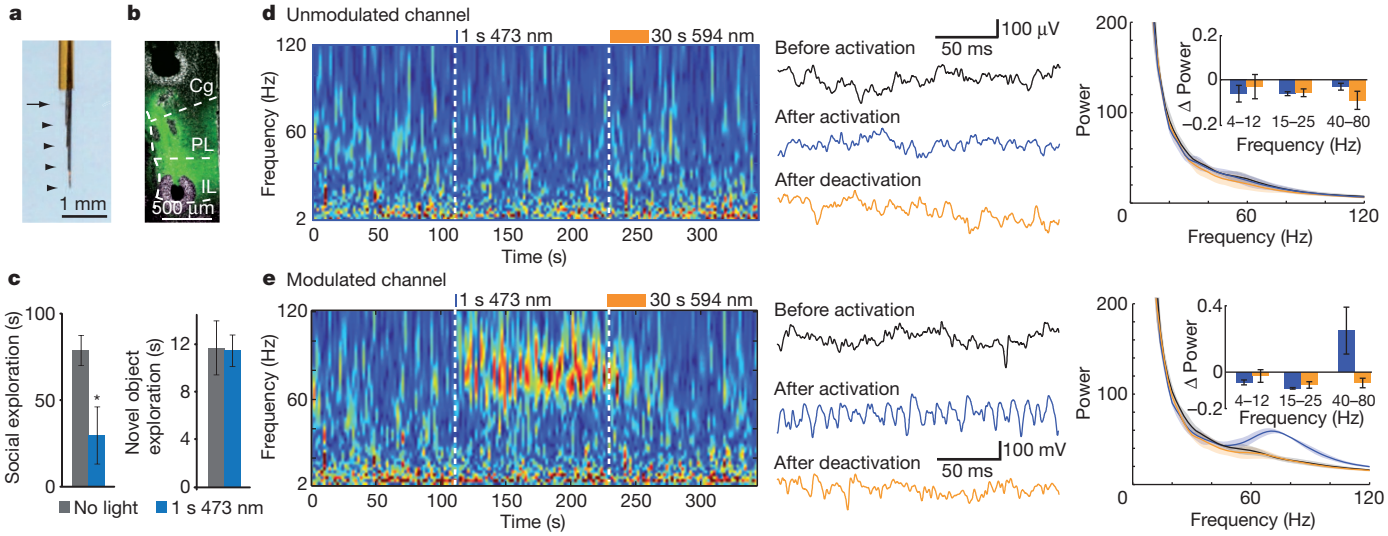

Figure 3 | Elevated cellular E/I balance in the mPFC drives baseline high frequency rhythmicity in freely moving, socially impaired mice. **a**, Implantable CMO for awake, behaving recordings in mouse M2 and PFC. Arrowheads indicate wire termination sites; arrow shows cleaved end of fibre-optic connector. **b**, Electolytic lesions mark the sites from which recordings were taken in a mouse expressing CaMKIIα::SSFO. **c**, Social (left) and novel object exploration (right) before (grey) and after (blue) activation with 473 nm light in mice used for CMO recordings ($n = 3$ mice). **d**, **e**, Local-field-potential wavelet spectrogram from a representative unmodulated channel (**d**) and a representative modulated channel (**e**). Example traces are shown for the baseline, activation and deactivation periods. Average wavelet spectra for the three indicated periods ($n = 5$ trials in 1 mouse) and population data (insets; $n = 3$ mice) are shown, demonstrating a specific increase in gamma rhythmicity on the modulated channel after SSFO activation in PFC pyramidal neurons. All bar graphs depict mean ± s.e.m. (*$P < 0.05$).

consistently increased in experiments where a 1 s 473 nm pulse was delivered during testing in the open field (Supplementary Fig. 8i and Supplementary Movie 3), during social exploration (Supplementary Fig. 8j and Supplementary Movie 5) and during novel object exploration (Supplementary Fig. 8k). Together, these data reveal that elevated rhythmic high-frequency activity, a disease correlate in clinical conditions, is elicited (along with social deficits) as a result of elevating cellular E/I balance in freely behaving mammals.

Development of potent redshifted control

We next sought to complement SSFO with a redshifted, fast-kinetic-response excitatory ChR for combinatorial control in the mPFC. Neurons expressing VChR1 showed weak expression (Fig. 4a) and small photocurrents (Supplementary Fig. 9a), consistent with previous findings[39]. Adding a Kir2.1 trafficking signal[47] (ts) to generate VChR1-ts–EYFP only modestly enhanced photocurrents (Supplementary Fig. 9a). We next systematically produced ChR1/VChR1 chimaeras and screened for enhanced membrane expression and photocurrent in HEK cells. We observed markedly improved membrane expression when VChR1 helices 1 and 2 were replaced with ChR1 homologues (Supplementary Fig. 9b) and selected two of these (fused at ChR1 Ala 145 or Trp 163) for further characterization (Supplementary Fig. 9a, c, d). In cultured neurons, the latter variant expressed more robustly and trafficked well to the membrane (Fig. 4a and Supplementary Fig. 9e, f) with enhanced peak photocurrents (888 ± 128 pA, $n = 11$ cells; $P < 0.0005$) compared with VChR1 (Supplementary Fig. 9a). The action spectrum remained redshifted (Supplementary Table 1 and Fig. 4d), while ion selectivity was similar to ChR2 and VChR1 (Supplementary Fig. 9g). The Kir2.1 trafficking sequence[47] further increased photocurrents (1104 ± 123 pA, $n = 12$ cells; Fig. 4e, Supplementary Fig. 9a and Supplementary Tables 1, 2). This ChR1/VChR1 chimaera contains no ChR2 sequence at all and is referred to here as C1V1.

Fast deactivation[37] of a redshifted opsin would be optimal for temporal and spectral separation from SSFO. However, C1V1-ts–EYFP photocurrents decayed >10-fold more slowly than those of ChR2, and indeed more slowly than those of VChR1 (Fig. 4c; τ_{off} 156 ± 12 ms and 132 ± 12 ms for C1V1-ts–EYFP ($n = 4$) and VChR1–EYFP ($n = 5$), respectively; Supplementary Table 1). To enhance photocurrent kinetics of C1V1, we used structural models to search the chromophore region[33,37] (Fig. 4b) for residues that might modulate photocycle kinetics, inactivation and blue absorption. We found that the E162T mutation (homologous to a ChETA mutation in ChR2) and the E122T mutation both significantly reduced τ_{off} (Fig. 4c). The combined E122T/E162T mutation synergistically enhanced photocurrent temporal precision while maintaining robust photocurrent sizes and reducing the residual shorter-wavelength response observed in VChR1 and C1V1(E162T) (Fig. 4c–e). Photocurrent sizes generally correlated with fluorescence intensity across constructs (Supplementary Fig. 9h), but C1V1(E122T/E162T) cells showed stronger photocurrents than ChR2(H134R) cells at equivalent fluorescence levels (Fig. 4f).

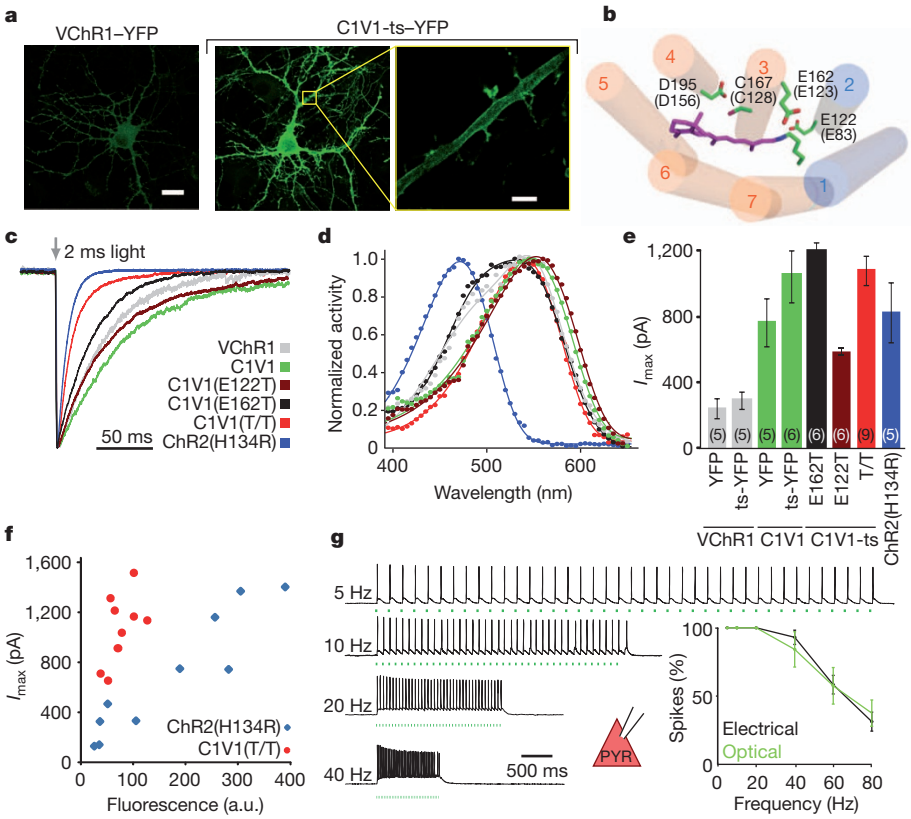

Figure 4 | Multistep engineering of a potent redshifted ChR. **a**, Confocal images of cultured hippocampal neurons transfected with VChR1–EYFP or C1V1-ts–EYFP under the control of the CaMKIIα promoter. Yellow box denotes region expanded in the last panel, showing dendritic membrane localization of C1V1-ts–EYFP. Scale bars: 20 μm (left, middle), 4 μm (right). **b**, Model of the C1V1 chromophore binding pocket, showing ChR1 helices in blue, VChR1 helices in orange, the retinal Schiff base (RSB) in purple, and key amino acid residues (with corresponding ChR2 numbering in parentheses and the modelled location of the SSFO mutations C128 and D156 shown for context). **c**, Representative traces and summary plot of channel closure time constant (τ_{off}) in cultured neurons expressing the indicated channelrhodopsins; traces are normalized to peak current. **d**, Action spectra collected for the indicated channelrhodopsins (colour code as in **c**). Photocurrents were collected with 2 ms light pulses in HEK293 cells. **e**, Mean peak photocurrents recorded in cultured neurons expressing the indicated channelrhodopsins in response to a 2 ms 542 nm light pulse. Colours are as indicated in **c**; numbers in brackets indicate *n*. **f**, Fluorescence–photocurrent relationship in ChR2(H134R) (blue) and C1V1(E122T/E162T) (red). a.u., arbitrary units. **g**, Acute slice recordings in prefrontal pyramidal neurons (PYR) expressing C1V1(E122T/E162T) and stimulated with 560 nm light pulse trains or current injections at the indicated frequencies. Summary graphs show light and current-evoked spike probability versus stimulation frequency ($n = 6$; $P > 0.4$ at all frequencies). All error bars indicate s.e.m.

Next we injected mice with AAV5-CaMKIIα::C1V1(E122T/E162T)-ts–EYFP virus in the mPFC and recorded from expressing neurons in acute slices. The frequency responses to trains of 2 ms light pulses or current injection pulses were indistinguishable (Fig. 4g; $n = 6$ cells in 2 slices), suggesting that in this case intrinsic cell properties and not opsin kinetics limit performance (Supplementary Fig. 10). We next found that with C1V1(E122T) (the most redshifted of all variants although somewhat slower than C1V1(E122T/E162T); Fig. 4d) reliable spiking with 630 nm light could be obtained (Supplementary Fig. 11). Lastly, using AAV5-CaMKIIα::C1V1(E122T/E162T) together with AAV5-EF1α::ChR2(H134R), we were able to differentially drive spiking in cortical pyramidal and PV neurons with 560 nm and 405 nm light, respectively (Supplementary Fig. 12). Combinatorial excitation was also possible with SSFO and C1V1, as peak frequencies of evoked rhythmic circuit activity generated in prefrontal cortical slices by C1V1 activation seemed to be shifted to higher frequencies by co-activation of SSFO in PV neurons (Supplementary Fig. 13). Furthermore, using C1V1 and ChR2 we were able to independently activate axons of two converging excitatory pathways (cortico-thalamic and thalamo-cortical) onto thalamic reticular nucleus neurons, observing that under these conditions the temporal coincidence of subthreshold synaptic inputs from each pathway can evoke spiking in target neurons (Supplementary Fig. 14). Together these results indicated that combinatorial control within intact tissue is enabled with these C1V1 variants.

Increased inhibition modulates behavioural deficits

In principle, an elevated E/I ratio could be achieved not only by increasing excitation but also by reducing inhibition, although this loss-of-function approach might be operative only under high baseline activity of the inhibitory cells (Supplementary Figs 6c, 15). However, a question salient to the elevated cellular E/I ratio hypothesis is whether adding an additional disruption in the form of increased inhibition could ameliorate behavioural deficits associated with elevated E/I balance. For this experiment, we first had to verify that combinatorial excitation could be feasible *in vivo*. We therefore explored combinatorial excitation of mPFC pyramidal and PV neurons *in vivo* with optrode recordings (Fig. 5a, left). To examine inhibitory effects of PV cell activity on pyramidal neuron spiking *in vivo*, we expressed CaMKIIα::C1V1(E122T/E162T) and DIO::ChR2(H134R) in the mPFC of PV::Cre mice. Using an optrode, we applied 5 Hz 405 nm pulses (to activate ChR2 in PV cells) followed by 5 Hz 561 nm pulses (to activate C1V1 in pyramidal neurons) while varying inter-pulse interval (Fig. 5a, right). The fidelity of green-light-evoked

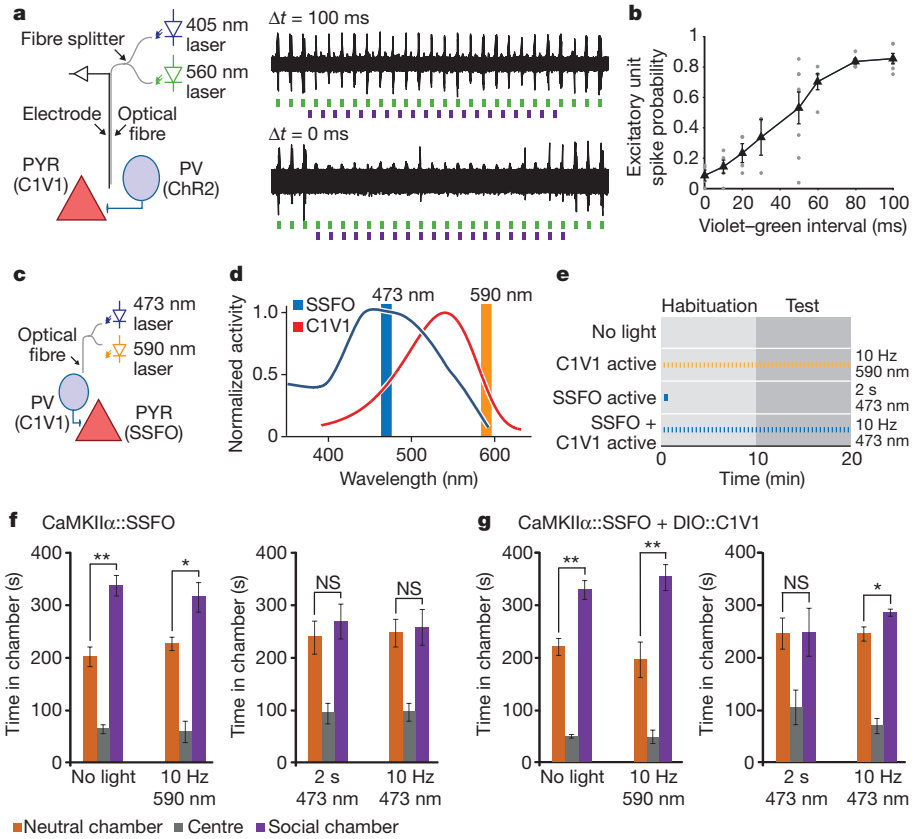

Figure 5 | Combinatorial optogenetics enables partial reversal of elevated E/I-balance social behaviour disruption. **a**, mPFC optrode recording in an anaesthetized PV::Cre mouse injected with CaMKIIα::C1V1(E162T)-ts–EYFP and Ef1a-DIO::ChR2–EYFP (diagram illustrates experimental setup). Violet (405 nm) light pulses are presented with variable delay (Δt) relative to green light pulses (example traces). **b**, Summary graph shows probability of green-light-evoked spikes with violet pulses preceding the green light pulses by the indicated delays. Individual points are from single recordings. Black line shows average for all recordings (>3 recording sites per bin). **c**, Experimental paradigm for SSFO activation in pyramidal neurons and C1V1 activation in PV neurons. **d**, Action spectra of SSFO (blue) and C1V1(E122T/E162T) (C1V1, red). Orange and blue vertical lines indicate stimulation wavelengths used in the experiments. **e**, Experiment design and pulse patterns; no-light control was used for baseline behaviour; 2 s 473 nm light for prolonged SSFO activation; 10 Hz 473 nm for co-activation of SSFO and C1V1; 10 Hz 590 nm for C1V1 activation. **f**, Mice expressing CaMKIIα::SSFO ($n = 7$) showed significant social preference at baseline, but exhibited social dysfunction after either 2 s 473 nm activation or during 10 Hz 473 nm activation. **g**, Mice expressing both CaMKIIα::SSFO and DIO-PV::C1V1 ($n = 7$) showed impaired social behaviour after a 2 s 473 nm pulse, but showed partially restored social behaviour during the 10 Hz 473 nm light stimulation. Activation of C1V1 alone with 10 Hz 590 nm pulses did not impair social behaviour. NS, not significant. Supplementary Fig. 16 shows normal social behaviour under all illumination conditions in YFP-expressing control cohorts. All error bars indicate s.e.m. (*$P < 0.05$; **$P < 0.005$).

events dropped as the inter-pulse interval decreased, with maximal excitatory responses observed with an interval of 100 ms (Fig. 5a, top trace) and responses were nearly abolished when light pulses were presented with sufficient synchrony (Fig. 5a, bottom trace; summary data in Fig. 5b). These data demonstrate combinatorial optogenetic control within an intact mammal.

We next leveraged combinatorial optogenetics *in vivo* to excite mPFC pyramidal cells with SSFO and PV neurons with C1V1 (E122T/E162T) in freely moving mice (Fig. 5c; referred to here as SSFO/C1V1 mice; $n = 7$). Control cohorts were injected with CaMKIIα::SSFO virus alone ($n = 7$) or with CaMKIIα::EYFP ($n = 8$). Mice were tested in the three-chamber social test under four different illumination paradigms, designed to examine behaviour with baseline properties, elevated excitatory tone, elevated inhibitory tone and co-elevated excitatory and inhibitory tone (Fig. 5d, e). All mice showed significant preference for the social chamber during baseline testing (Fig. 5f, g and Supplementary Fig. 16; CaMKIIα::SSFO mice, $P = 0.0002$; SSFO/C1V1 mice, $P = 0.0014$; CaMKIIα::EYFP mice, $P = 0.0029$). Under pulsed laser light at 590 nm, all mice showed significant preference for the social chamber (Fig. 5f, g and Supplementary Fig. 16; CaMKIIα::SSFO mice, $P = 0.02$; SSFO/C1V1 mice, $P = 0.0048$; CaMKIIα::EYFP mice, $P = 0.039$). After a 2 s 473 nm pulse given at the beginning of the test, neither the CaMKIIα::SSFO nor the SSFO/C1V1 mice preferred the social chamber (Fig. 5f, g and Supplementary Fig. 16; $P = 0.52$ and $P = 0.96$, respectively). Lastly, we sought to ameliorate the behaviour deficit by compensating cellular E/I balance, co-activating SSFO in excitatory cells and C1V1(E122T/E162T) in inhibitory cells by pulsing 10 Hz 473 nm light throughout the test period (Fig. 5f, g). CaMKIIα::SSFO mice (with no C1V1(E122T/E162T) and thus experiencing purely cellular E/I balance elevation) showed no significant preference for the social chamber (Fig. 5f; $P = 0.81$); in contrast, despite the sparseness of the PV population and incomplete transduction under these conditions (Supplementary Fig. 2) SSFO/C1V1 showed modest but significant preference for the social chamber (Fig. 5g; $P = 0.026$). Control CaMKIIα::EYFP mice significantly preferred the social chamber under both the 2 s 473 nm and the 10 Hz 473 nm paradigms (Supplementary Fig. 16). Together, this series of experiments indicate that social deficits seen with elevated mPFC cellular E/I balance may be partially reduced by restoring balance with increased inhibitory tone.

Discussion

Several lines of evidence have indicated the involvement of elevated cellular E/I balance in the aetiology of medication-unresponsive social and information-processing impairments in autism and schizophrenia, although it has been unclear if such an effect would operate on the acute or chronic timescale[3,9,10,23,28,48]. Moreover, the tight interplay and complexity of excitation and inhibition within cortical microcircuitry have precluded the direct investigation of cell- and circuit-level effects of changes in cellular E/I balance; for example, cell-specific pharmacological agents are lacking, and homeostatic processes can occur downstream of synaptic and intrinsic excitability alterations. We therefore sought to investigate the effects of this altered cellular E/I balance on the acute timescale and quantify the effects on information transmission, network activity and animal behaviour. To stably modulate neural activity in awake animals, we produced an SSFO that enabled combined spectral/temporal separation when used together with red-shifted opsins (C1V1 variants), developed as chimaeras along with combinatorial mutagenesis of the chromophore region to enhance potency, kinetics and spectral properties.

With these new tools, we obtained causal support for the elevated cellular E/I balance hypothesis, and identified circuit-physiology manifestations of the resulting social dysfunction. SSFO activation in prefrontal cortical excitatory (but not inhibitory) neurons led to profound, yet reversible, impairments in social function and cognition without motor abnormalities or increased anxiety. To understand more fully the elevated E/I state, we probed both *in vitro* and *in vivo* the underlying circuit-physiology manifestations. Despite the complexity resulting from the broad range of circuit phenomena that a cellular E/I balance modulation could initiate, we found that cellular E/I balance elevation, but not reduction under these conditions, altered the transfer functions of principal neurons in a way that quantitatively impaired information transmission within cortical circuitry. The effects of elevated E/I balance on social behaviour showed evidence of specificity for the PFC, as increasing the E/I ratio in primary visual cortex did not impair social behaviour. The PFC network, with its extensive subcortical connectivity, might therefore be particularly susceptible to eliciting psychiatric symptom-related effects in the setting of subtle changes in E/I balance, a notion that is supported by observed alterations in PFC inhibitory markers associated with psychiatric disease[12,13,48–50] and the altered PFC rhythmicity observed in autistic individuals[20]. And using spectrotemporal separation of the activity of SSFO and C1V1, we found that increased cellular inhibition moderately ameliorated the social behaviour deficits in mice that had been subjected to elevation of cellular E/I balance.

We also identified correspondence between a clinical marker of disease states linked to social dysfunction (elevated baseline gamma power) and electrophysiological findings during free behaviour in the elevated cellular E/I state. We found that the elevated E/I state was associated with robust, stable high-frequency power in the 30–80 Hz range generated by and manifested within the regions directly experiencing elevated cellular E/I balance. Stimulus-evoked gamma oscillations had previously been shown to be important for refining information flow through cortical circuitry[32], but high baseline (unevoked) gamma oscillations may interfere with cortical function and contribute to disease states[20,21]. Together, these temporally delimited, cell-type-specific optogenetic manipulations (although fully capable of causing either acute or chronic changes in complex local circuit processing and input–output relationships) distinguish direct real-time effects of cellular E/I balance changes *in vivo* from the many possible developmental and structural alterations that could occur with more chronic interventions[25–29]. Despite the complexity of homeostatic processes that contribute to behavioural phenotypes in genetic models, our data are consistent with the E/I balance hypothesis and with recent reports of impaired social function and learning in mouse models of Rett syndrome[28,29]. In sum, these findings may represent a step towards understanding the pathophysiology of social and information-processing dysfunction, and despite the complexity of cortical processing, together provide causal support for the cellular E/I balance elevation hypothesis of severe psychiatric disease symptomatology on the cellular, circuit and behavioural levels.

METHODS SUMMARY

C1V1 was cloned by overlap extension PCR, fusing the N-terminal sequence of the *Chlamydomonas reinhardtii* ChR1 coding sequence[40] with the C-terminal sequence of *Volvox carteri* ChR1[39]. SSFO mutants were generated by site-directed mutagenesis of the humanized ChR2 sequence. Constructs were cloned into the pLenti or pAAV-MCS backbone under control of the CaMKIIα promoter or using a double-floxed inverted open-reading frame (ORF) Cre-dependent backbone[32]. Maps and clones are available at http://www.optogenetics.org.

Virus was stereotactically injected 2–3 weeks before physiological experiments or behavioural testing. Optrode recordings in anaesthetized mice were conducted as described[41] using a dual-laser system with either 473 nm and 561 nm lasers for SSFO experiments or 405 nm and 561 nm lasers for combinatorial excitation experiments with ChR2 and C1V1.

Recordings in behaving mice were performed using custom-built 4-microwire arrays attached to an optical fibre. Arrays were designed to sample from a large anatomical volume including transduced and untransduced tissue. Data were analysed in Matlab, using custom software; spectral analysis was performed using the wavelet method[32].

Received 17 September 2010; accepted 10 July 2011.
Published online 27 July 2011.

1. Pardo, C. A. & Eberhart, C. G. The neurobiology of autism. *Brain Pathol.* **17,** 434–447 (2007).

2. O'Donovan, M. C., Craddock, N. J. & Owen, M. J. Genetics of psychosis; insights from views across the genome. *Hum. Genet.* **126,** 3–12 (2009).
3. Südhof, T. C. Neuroligins and neurexins link synaptic function to cognitive disease. *Nature* **455,** 903–911 (2008).
4. Patterson, P. H. Modeling autistic features in animals. *Pediatr. Res.* **69,** 34R–40R (2011).
5. Walsh, T. *et al.* Rare structural variants disrupt multiple genes in neurodevelopmental pathways in schizophrenia. *Science* **320,** 539–543 (2008).
6. Markram, K. & Markram, H. The intense world theory—a unifying theory of the neurobiology of autism. *Front. Hum. Neurosci.* **4,** 224 (2010).
7. Vattikuti, S. & Chow, C. C. A computational model for cerebral cortical dysfunction in autism spectrum disorders. *Biol. Psychiatry* **67,** 672–678 (2010).
8. Kehrer, C., Maziashvili, N., Dugladze, T. & Gloveli, T. Altered excitatory-inhibitory balance in the NMDA-hypofunction model of schizophrenia. *Front. Mol. Neurosci.* **1,** 6 (2008).
9. Rubenstein, J. L. Three hypotheses for developmental defects that may underlie some forms of autism spectrum disorder. *Curr. Opin. Neurol.* **23,** 118–123 (2010).
10. Rubenstein, J. L. & Merzenich, M. M. Model of autism: increased ratio of excitation/inhibition in key neural systems. *Genes Brain Behav.* **2,** 255–267 (2003).
11. Gogolla, N. *et al.* Common circuit defect of excitatory-inhibitory balance in mouse models of autism. *J. Neurodevelop. Disord.* **1,** 172–181 (2009).
12. Hashimoto, T. *et al.* Conserved regional patterns of GABA-related transcript expression in the neocortex of subjects with schizophrenia. *Am. J. Psychiatry* **165,** 479–489 (2008).
13. Hashimoto, T. *et al.* Gene expression deficits in a subclass of GABA neurons in the prefrontal cortex of subjects with schizophrenia. *J. Neurosci.* **23,** 6315–6326 (2003).
14. Belforte, J. E. *et al.* Postnatal NMDA receptor ablation in corticolimbic interneurons confers schizophrenia-like phenotypes. *Nature Neurosci.* **13,** 76–83 (2010).
15. Blatt, G. J. *et al.* Density and distribution of hippocampal neurotransmitter receptors in autism: an autoradiographic study. *J. Autism Dev. Disord.* **31,** 537–543 (2001).
16. Bourgeron, T. A synaptic trek to autism. *Curr. Opin. Neurobiol.* **19,** 231–234 (2009).
17. Belmonte, M. K., Gomot, M. & Baron-Cohen, S. Visual attention in autism families: 'unaffected' sibs share atypical frontal activation. *J. Child Psychol. Psychiatry* **51,** 259–276 (2010).
18. Gomot, M., Belmonte, M. K., Bullmore, E. T., Bernard, F. A. & Baron-Cohen, S. Brain hyper-reactivity to auditory novel targets in children with high-functioning autism. *Brain* **131,** 2479–2488 (2008).
19. Dichter, G. S., Felder, J. N. & Bodfish, J. W. Autism is characterized by dorsal anterior cingulate hyperactivation during social target detection. *Soc. Cogn. Affect. Neurosci.* **4,** 215–226 (2009).
20. Orekhova, E. V. *et al.* Excess of high frequency electroencephalogram oscillations in boys with autism. *Biol. Psychiatry* **62,** 1022–1029 (2007).
21. Rojas, D. C., Maharajh, K., Teale, P. & Rogers, S. J. Reduced neural synchronization of gamma-band MEG oscillations in first-degree relatives of children with autism. *BMC Psychiatry* **8,** 66 (2008).
22. Gillberg, C. & Billstedt, E. Autism and Asperger syndrome: coexistence with other clinical disorders. *Acta Psychiatr. Scand.* **102,** 321–330 (2000).
23. Canitano, R. Epilepsy in autism spectrum disorders. *Eur. Child Adolesc. Psychiatry* **16,** 61–66 (2007).
24. Rippon, G., Brock, J., Brown, C. & Boucher, J. Disordered connectivity in the autistic brain: challenges for the ''new psychophysiology''. *Int. J. Psychophysiol.* **63,** 164–172 (2007).
25. Dani, V. S. *et al.* Reduced cortical activity due to a shift in the balance between excitation and inhibition in a mouse model of Rett syndrome. *Proc. Natl Acad. Sci. USA* **102,** 12560–12565 (2005).
26. Etherton, M. R., Blaiss, C. A., Powell, C. M. & Sudhof, T. C. Mouse neurexin-1α deletion causes correlated electrophysiological and behavioral changes consistent with cognitive impairments. *Proc. Natl Acad. Sci. USA* **106,** 17998–18003 (2009).
27. Tabuchi, K. *et al.* A neuroligin-3 mutation implicated in autism increases inhibitory synaptic transmission in mice. *Science* **318,** 71–76 (2007).
28. Chao, H. T. *et al.* Dysfunction in GABA signalling mediates autism-like stereotypies and Rett syndrome phenotypes. *Nature* **468,** 263–269 (2010).
29. Moretti, P. *et al.* Learning and memory and synaptic plasticity are impaired in a mouse model of Rett syndrome. *J. Neurosci.* **26,** 319–327 (2006).
30. Rinaldi, T., Perrodin, C. & Markram, H. Hyper-connectivity and hyper-plasticity in the medial prefrontal cortex in the valproic acid animal model of autism. *Front. Neural Circuits* **2,** 4 (2008).
31. Adamantidis, A. R., Zhang, F., Aravanis, A. M., Deisseroth, K. & de Lecea, L. Neural substrates of awakening probed with optogenetic control of hypocretin neurons. *Nature* **450,** 420–424 (2007).
32. Sohal, V. S., Zhang, F., Yizhar, O. & Deisseroth, K. Parvalbumin neurons and gamma rhythms enhance cortical circuit performance. *Nature* **459,** 698–702 (2009).
33. Berndt, A., Yizhar, O., Gunaydin, L. A., Hegemann, P. & Deisseroth, K. Bi-stable neural state switches. *Nature Neurosci.* **12,** 229–234 (2009).
34. Diester, I. *et al.* An optogenetic toolbox designed for primates. *Nature Neurosci.* **14,** 387–397 (2011).
35. Bamann, C., Gueta, R., Kleinlogel, S., Nagel, G. & Bamberg, E. Structural guidance of the photocycle of channelrhodopsin-2 by an interhelical hydrogen bond. *Biochemistry* **49,** 267–278 (2010).
36. Yizhar, O., Fenno, L., Davidson, T. J., Mogri, M. & Deisseroth, K. Optogenetics in neural systems. *Neuron* **71,** 9–34 (2011).
37. Gunaydin, L. A. *et al.* Ultrafast optogenetic control. *Nature Neurosci.* **13,** 387–392 (2010).
38. Wen, L. *et al.* Opto-current-clamp actuation of cortical neurons using a strategically designed channelrhodopsin. *PLoS ONE* **5,** e12893 (2010).
39. Zhang, F. *et al.* Red-shifted optogenetic excitation: a tool for fast neural control derived from *Volvox carteri*. *Nature Neurosci.* **11,** 631–633 (2008).
40. Nagel, G. *et al.* Channelrhodopsin-1: a light-gated proton channel in green algae. *Science* **296,** 2395–2398 (2002).
41. Gradinaru, V. *et al.* Targeting and readout strategies for fast optical neural control *in vitro* and *in vivo*. *J. Neurosci.* **27,** 14231–14238 (2007).
42. Lind, S. E. & Bowler, D. M. Episodic memory and episodic future thinking in adults with autism. *J. Abnorm. Psychol.* **119,** 896–905 (2010).
43. D'Argembeau, A., Raffard, S. & Van der Linden, M. Remembering the past and imagining the future in schizophrenia. *J. Abnorm. Psychol.* **117,** 247–251 (2008).
44. Ni, A. M. & Maunsell, J. H. Microstimulation reveals limits in detecting different signals from a local cortical region. *Curr. Biol.* **20,** 824–828 (2010).
45. Moy, S. S. *et al.* Sociability and preference for social novelty in five inbred strains: an approach to assess autistic-like behavior in mice. *Genes Brain Behav.* **3,** 287–302 (2004).
46. Wilson, T. W., Rojas, D. C., Reite, M. L., Teale, P. D. & Rogers, S. J. Children and adolescents with autism exhibit reduced MEG steady-state gamma responses. *Biol. Psychiatry* **62,** 192–197 (2007).
47. Gradinaru, V. *et al.* Molecular and cellular approaches for diversifying and extending optogenetics. *Cell* **141,** 154–165 (2010).
48. Lewis, D. A., Hashimoto, T. & Volk, D. W. Cortical inhibitory neurons and schizophrenia. *Nature Rev. Neurosci.* **6,** 312–324 (2005).
49. Lewis, D. A., Volk, D. W. & Hashimoto, T. Selective alterations in prefrontal cortical GABA neurotransmission in schizophrenia: a novel target for the treatment of working memory dysfunction. *Psychopharmacology (Berl.)* **174,** 143–150 (2004).
50. Lisman, J. E. *et al.* Circuit-based framework for understanding neurotransmitter and risk gene interactions in schizophrenia. *Trends Neurosci.* **31,** 234–242 (2008).

Supplementary Information is linked to the online version of the paper at www.nature.com/nature.

Acknowledgements We thank the K.D., P.H. and J.R.H. laboratories for discussions on the manuscript. We are grateful to S. Pak, Z. Chen and C. Perry for technical assistance. O.Y. is supported by the Human Frontier Science Program. L.E.F. is supported by the Stanford MSTP program. P.H. is supported by the DFG (HE3824/9-1 and 17-1, Cluster of Excellence: Unifying Concepts in Catalysis), and K.D. by NIMH, NIDA, NINDS, the DARPA REPAIR program, CIRM and the Yu, Woo, Snyder and Keck Foundations.

Author Contributions O.Y., M.P., F.S. and C.R. designed and cloned all DNA constructs; O.Y. and L.E.F. contributed to all neuronal electrophysiology and behavioural experiments; T.J.D. designed the CMO implant; I.G. and J.F. contributed to behaviour and histology experiments; D.J.O. and V.S.S. contributed to slice electrophysiology and mutual information analysis; K.S. and R.F. performed spectroscopy experiments; M.P. and F.S. performed HEK cell experiments; P.H. analysed and supervised spectroscopy and HEK cell work; J.T.P. and J.R.H. conducted and analysed, and J.R.H. supervised, thalamic slice experiments. K.D. supervised all aspects of the project and O.Y., L.E.F. and K.D. wrote the manuscript.

Author Information Reprints and permissions information is available at www.nature.com/reprints. The authors declare no competing financial interests. Readers are welcome to comment on the online version of this article at www.nature.com/nature. Correspondence and requests for materials should be addressed to O.Y. (ofer.yizhar@weizmann.ac.il), P.H. (hegemape@rz.hu-berlin.de) or K.D. (deissero@stanford.edu).